Journal of Molecular Liquids 277 (2019) 175–180

Contents lists available at ScienceDirect

Journal of Molecular Liquids

journal homepage: www.elsevier.com/locate/molliq

Flake size-dependent adsorption of graphene oxide aerogel

Soon Poh Lee [a], Gomaa A.M. Ali [a,b], H. Algarni [c,d], Kwok Feng Chong [a,*]

[a] Faculty of Industrial Sciences & Technology, Universiti Malaysia Pahang, Gambang, 26300 Kuantan, Malaysia
[b] Chemistry Department, Faculty of Science, Al–Azhar University, Assiut 71524, Egypt
[c] Department of Physics, Faculty of Sciences, King Khalid University, P. O. Box 9004, Abha, Saudi Arabia
[d] Research Center for Advanced Materials Science (RCAMS), King Khalid University, Abha 61413, P. O. Box 9004, Saudi Arabia

ARTICLE INFO

Article history:
Received 14 November 2018
Received in revised form 13 December 2018
Accepted 18 December 2018
Available online 23 December 2018

Keywords:
Aerogel
Graphene
Hydroxyl groups
Sheet size
Water treatment

ABSTRACT

In this work, the flake size-dependent adsorption kinetics of graphene oxide (GO) aerogel is studied. GO in different flake sizes are produced by sonication prior to the preparation of aerogel through freeze-dry method. The structural characterizations reveal that GO aerogel with smaller flake size possesses higher surface area and higher intensity of edge-plane oxygen functionalities. These provide more adsorption sites and active sites for heavy metal ions adsorption. Adsorption study reveals the higher Fe^{3+} ions adsorption capacity as well as uptake rate on GO aerogel with smaller flake size. The adsorption kinetic obeys the pseudo-second-order kinetic model which indicates the chemisorption is the rate-determining step. Adsorption isotherms of GO aerogel on Fe^{3+} ions show highest Langmuir adsorption capacity of 133.3 mg/g and render it to be a potential material for heavy metal ions removal in wastewater treatment.

1. Introduction

Water quality is a concern for global organization and government. World Health Organization (WHO) works on the acceptability ions content to determine the acceptable water quality [1]. In 2015, United Nations Children's Fund (UNICEF) and WHO had run an assessment on the sanitation and drinking water which reported about 663 million global citizens still lack of clean water resource which is a crucial issue in the world [2]. Global industrialization could be the culprit for such crisis as the industrial wastes in the form of organic pollutants or metals ions are directly disposed to the environment [3]. Iron ions (Fe^{3+}) is one of the heavy metals ions if it is consumed in excess amount, can cause severe diseases, such as Eales disease, Alzheimer's disease and Parkinson's disease [4,5]. Hence, the high levels of Fe^{3+} ions in water will be an apprehension.

Different methods were reported for Fe^{3+} removals such as ion exchange, dialysis sac, electrochemical oxidation, precipitation and adsorption [6–9]. Among them, adsorption is the most cost-effective approach with good performance. Activated carbon is commonly found as one of the water treatment adsorbents due to its low-cost [10–12]. However, there are some limitations of the activated carbon used for water treatment. It suffers from low adsorption capacity (2.50, 7.74, 3.08, 6.69 and 2.83 mg/g for Ni^{2+}, Co^{2+}, Cd^{2+}, Pb^{2+}, Cu^{2+} and Cr^{3+}, respectively [13]) and low heavy metal removal efficiency due to the limited specific sites for retaining heavy metal ions [14,15]. In this context, graphene is one of the materials that is investigated to replace activated carbon. This is due to its structure that shows nanosorbent properties and is able to associate with heavy metals ions at even ppb levels [16]. Graphene and graphene oxide (GO) were used widely for heavy metal ions removal [17,18]. GO showed adsorption capacity of 116.35, 35.6 and 27.3 mg/g for Co^{2+}, Ni^{2+} and Fe^{3+}, respectively [19,20]. GO aerogel is a form of adsorbent that has promising adsorption capacity [21]. Its interconnected network structure with pores and high surface area are the major properties contributing to this outstanding adsorption result [14,22]. GO aerogel is proven to be able to remove Cu^{2+} ions in aqueous solution with uptake capacity up to 19.65 mg/g [23]. GO aerogel can be facilely produced by freeze-drying GO suspension. Therefore, GO flake size is vital in contributing to its aerogel physicochemical properties. To the best of our knowledge, there is no studies report on the effect of GO flake sizes in aerogel for the metal ions adsorption. The current work reports on the effect of flake size in GO aerogel for Fe^{3+} (as heavy metal ion model) adsorption and its adsorption kinetics is elucidated. Its adsorption understanding is expected to stimulate GO aerogel design to facilitate heavy metal ions removal.

2. Experimental section

2.1. Materials

Graphite flake (+100 mesh) was purchased from Graphene Supermarket. Potassium peroxodisulfate ($K_2S_2O_8$, Sigma-Aldrich), phosphorus pentoxide (P_2O_5, Sigma-Aldrich), sulfuric acid (95.0–98.0% H_2SO_4,

* Corresponding author.
E-mail address: ckfeng@ump.edu.my (K.F. Chong).

https://doi.org/10.1016/j.molliq.2018.12.097
0167-7322/

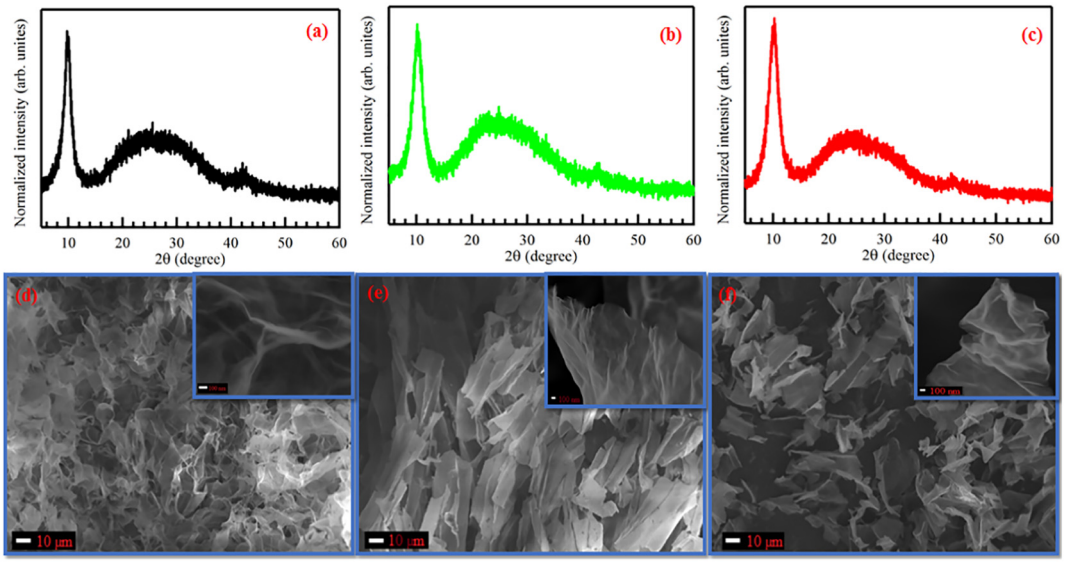

Fig. 1. (a, b and c) XRD patterns and (d, e and f) FESEM images for GO 0 h, GO 4 h and GO 12 h aerogel, respectively. The insets show the high magnification images.

J.T. Baker), potassium permanganate ($KMnO_4$, R&M Chemicals), hydrogen peroxide solution (30% H_2O_2, HmbG Chemicals), hydrochloric acid (37% HCl, Merck), iron(III) chloride hexahydrate ($FeCl_3 \cdot 6H_2O$, Merck) and liquid nitrogen (N_2) were used without any further purification or otherwise stated.

2.2. Preparation of size-controlled graphene oxide aerogel

Graphene oxide (GO) was synthesized using a modified Hummers' method [24,25]. Firstly, graphite flake (4 g) was added into H_2SO_4 (60 mL) followed by $K_2S_2O_8$ (6 g) and P_2O_5 (6 g) under stirring. The mixture was heated at 80 °C in an oil bath for 6 h prior to cooling to room temperature. Then, the mixture was diluted with 2 L of deionized water and washed until neutral pH with deionized water. Pre-oxidized graphite was obtained after the residue dried in vacuum. It was then sonicated for 0, 4 and 12 h to obtain different flake sizes. After that, the pre-oxidized graphite was oxidized using $KMnO_4$ (35 g) with H_2SO_4 (300 mL) as solvent at 35 °C in an oil bath for 4 h under stirring. The mixture was diluted with deionized water (700 mL) followed by H_2O_2 (100 mL) addition. Next, 1:10 HCl (2 L) was added to the mixture and washed using centrifugation with excess deionized water until neutral in pH. The resulting material was solidified at −80 °C followed by freeze-drying to obtain graphite oxide. Graphite oxide dispersions (8 mg/mL) was briefly sonicated to exfoliate into graphene oxide (GO).

The GO dispersion was later centrifuged at 500 rpm for 10 min and the supernatant was then dipped into liquid N_2 with the whole tube covered by styrofoam except bottom tip covered by stainless-steel plate to freeze the GO dispersion [23]. Different GO aerogel samples were obtained after 48 h of freeze-drying from the frozen GO dispersion. According to the sonication time during GO preparation, the GO aerogel samples were termed as GO 0 h, GO 4 h and GO 12 h to indicate the no sonication, 4 h sonication and 12 h sonication, respectively.

2.3. Characterizations techniques

Crystal structure and flake size of GO aerogel were analyzed using X-ray diffraction (XRD) with Rigaku Miniflex II for 2θ from 3 to 80°. Fourier-transform infrared (FTIR) measurements were carried out for the frequency from 400 to 4000 cm^{-1} using PerkinElmer Spectrum 100 spectrophotometer. The morphology of GO aerogel was observed with JEOL JSM-7800F field emission scanning electron microscope (FESEM). The surface area of GO aerogel was studied using micromeritics ASAP 2020 Brunauer–Emmett–Teller (BET) surface area and porosity analyzer with N_2 gas at 77 K.

2.4. Adsorption experiments

Standardized Fe^{3+} was prepared from $FeCl_3.6H_2O$ stock solution (0.1 mg/mL) with further dilution for desired concentration. In the adsorption experiment, 12 mg of GO aerogel was dipped into 20 mL Fe^{3+} solution. The solution was taken out at a certain time period and filtered to measure the Fe^{3+} concentration using Tecan Infinite M200 PRO with UV–Vis measurement at 294 nm. The adsorbed quantity (q_e) and the removal (%) of Fe^{3+} at the equilibrium were calculated using Eqs. (1) and (2) [18,26–28]:

$$q_e = \frac{(C_o - C_e)V}{W} \quad (1)$$

$$Removal\ (\%) = \frac{(C_o - C_e)}{C_o} \times 100 \quad (2)$$

where C_o is the initial Fe^{3+} concentration (mg/mL); C_e is the equilibrium Fe^{3+} concentration (mg/mL); V is the volume of the solution (mL) and W is the weight of the adsorbent (g).

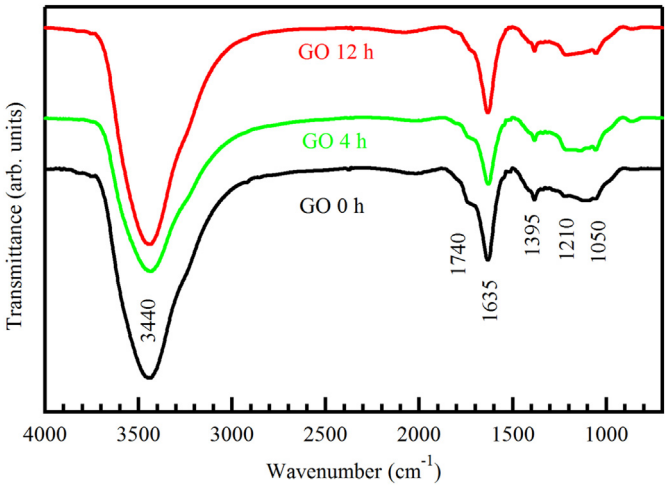

Fig. 2. FTIR spectra for GO aerogel prepared at different sonication times.

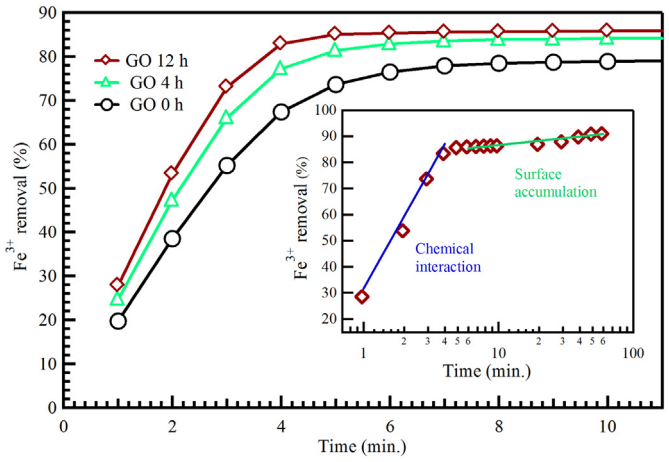

Fig. 3. Fe^{3+} ions uptake rate on different GO aerogel samples. The inset shows the two steps in the adsorption process.

3. Results and discussion

3.1. Structural and morphological analyses

Fig. 1a–c shows the XRD patterns of three different GO aerogel samples (GO 0 h, GO 4 h and GO 12 h). There is a significant peak observed for all GO aerogel samples at ca. $2\theta = 10.27°$, which indicates the expanded interlayer spacing of GO (9.05 Å) as compared to graphite (3.7 Å) [29,30] and reduced GO (4.0 Å) [31]. The expansion is due to the intercalation of oxygenated groups in between graphite planes [32]. The increase in the sonication time leads to an increase in full width at half maximum (FWHM), where the values are obtained to be 1.54, 2.27 and 2.47° for GO 0 h, GO 4 h and GO 12 h, respectively. It is inferred that longer sonication time produces disordered stacking in graphene oxide, which could be attributed to the smaller flake size. The average crystallite size is estimated by using Scherrer's equation. The obtained crystallite sizes are 5.18, 3.51 and 3.23 nm for GO 0 h, GO 4 h and GO 12 h, respectively. As expected, longer sonication time causes greater fragmentation in GO, and subsequently produces GO aerogel with smaller flake size. The peak broadening at $2\theta = 26.5$ ° for all GO aerogel samples is attributed to this incomplete oxidation of graphite precursor. It is worth noting that this incomplete oxidation of graphite is crucial in retaining the integrity of GO aerogel where it remained in its aerogel form throughout the adsorption studies.

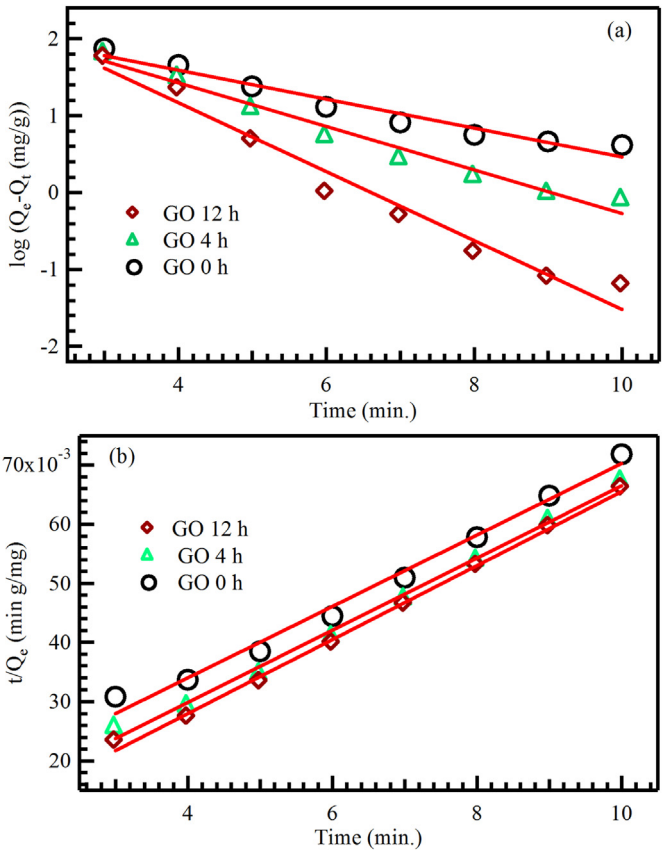

Fig. 5. (a) Pseudo-first-order and (b) pseudo-second-order for Fe^{3+} ions adsorption onto GO aerogel.

The GO aerogel samples morphology was investigated using FESEM as shown in Fig. 1d–f. The GO aerogel samples exhibit 3D interconnected network structure formed by randomly oriented GO flakes. A distinctive difference can be observed where GO with smaller flake size (GO 12 h) forms the aerogel with less compact structure while GO with larger flake size (GO 0 h) forms the compact aerogel structure. Such compact structure of GO 0 h signifies the lower surface area which

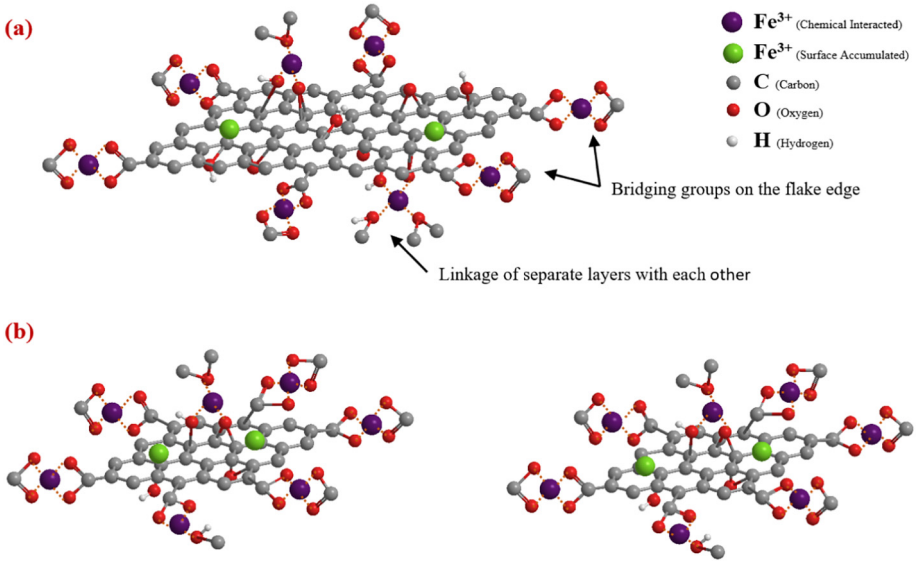

Fig. 4. Schematic diagram of Fe^{3+} ions adsorption at GO aerogel with (a) larger flakes size (b) smaller flakes size.

Table 1
Parameters of two kinetic models for Fe^{3+} adsorption onto GO aerogel.

Kinetic models	Parameters	GO 0 h	GO 4 h	GO 12 h
Pseudo-first-order	q_{cal} (mg/g)	67.46	159.00	283.30
	k_1 (min^{-1})	0.2445	0.6039	1.0466
	R^2	0.9559	0.9932	0.9690
	Δq%	74.86	9.24	123.76
Pseudo-second-order	q_{cal} (mg/g)	153.14	152.21	147.28
	k_2 (g/mg min)	0.0133	0.0093	0.0059
	R^2	0.9887	0.9949	0.9972
	Δq%	9.68	2.56	3.64
	q_{exp} (mg/g)	147.33	152.50	159.50

could limit the adsorption capacity. It is well corroborated by the surface area analysis (N_2 adsorption-desorption isotherm, Fig. S1) where GO 0 h merely shows a surface area of 16.9 m^2/g. With increasing sonication time in the preparation of GO aerogel, the surface area is increased from 89.1 m^2/g (GO 4 h) to 330.7 m^2/g (GO 12 h). The higher surface area of GO 12 h is crucial to provide more binding sites for the adsorption. In addition, the larger flakes in GO 0 h tend to roll up due to the intraplanar interaction and subsequently reduce active sites for adsorption. This is well supported by the FESEM at higher magnification (insets of Fig. 1d–f) where the single flake in GO 0 h shows multiple folding but single flake in GO 12 h only shows the crumpled structure and retains most of the binding sites for adsorption.

The oxygen functionalities of GO aerogel samples were studied by FTIR (Fig. 2). The bands at ca. 1395, 1220 and 1060 cm^{-1} are related to the vibrational bands of carboxyl, epoxy and alkoxy, respectively, confirm the basal plane oxygen functionalities of GO [30]. The absorption band at ca. 1740 cm^{-1} is due to the C═O stretching in COOH groups [30]. Previous studies report that the edge plane oxygen functionalities of GO could interact better with the heavy metal ions [33,34]. In this study, the hydroxyl group quantification is performed to estimate the amount of edge-plane oxygen functionalities as most of the hydroxyl groups are found at the edge of GO sheets [35]. The FTIR peak area values are 1122.57, 3790.49 and 5229.93 for GO 0 h, GO 4 h and GO 12 h, respectively. It can be clearly seen that GO aerogel with smaller flake size (GO 12 h) possesses higher amount of edge-plane oxygen functionalities (hydroxyl groups), which is crucial for interacting with heavy metal ions in adsorption study.

3.2. Adsorption process

The flake size effect in GO aerogel adsorption was investigated by studying its Fe^{3+} removal in the solution for 60 mins. The total Fe^{3+} ions removal by GO aerogel is increased with the order of GO 0 h, GO 4 h and GO 12 h (83.55, 86.48 and 90.45%, respectively), which implies the GO aerogel with smaller flakes size has higher adsorption towards Fe^{3+} ions.

The Fe^{3+} ions uptake rate by GO aerogel is shown in Fig. 3. It can be seen that all GO aerogel samples exhibit a high uptake rate at the beginning (first 6 min.) of contact to the Fe^{3+} solution. This is due to the adsorption sites of the GO aerogel are free of adsorbates which favor the contact with Fe^{3+} ions. The adsorption reaches a plateau after 6 min with a small increment of the capacity until the end of the adsorption study. Coherent to the total Fe^{3+} ions removal findings, the uptake rate is increased in the order of GO 0 h, GO 4 h and GO 12 h. Based on the Fe^{3+} uptake rate, the process of Fe^{3+} ions adsorption by GO aerogel is divided into two steps: (1) chemical interaction between Fe^{3+} ions and GO functional groups (fast rate) and (2) surface accumulation of Fe^{3+} ions on the GO flakes (slow rate). Inset of Fig. 3 shows the Fe^{3+} removal rate for GO 12 h where 86% of Fe^{3+} is removed by chemical interaction while only 4.5% of Fe^{3+} is removed by surface accumulation process. It points out the importance of chemical interaction in the

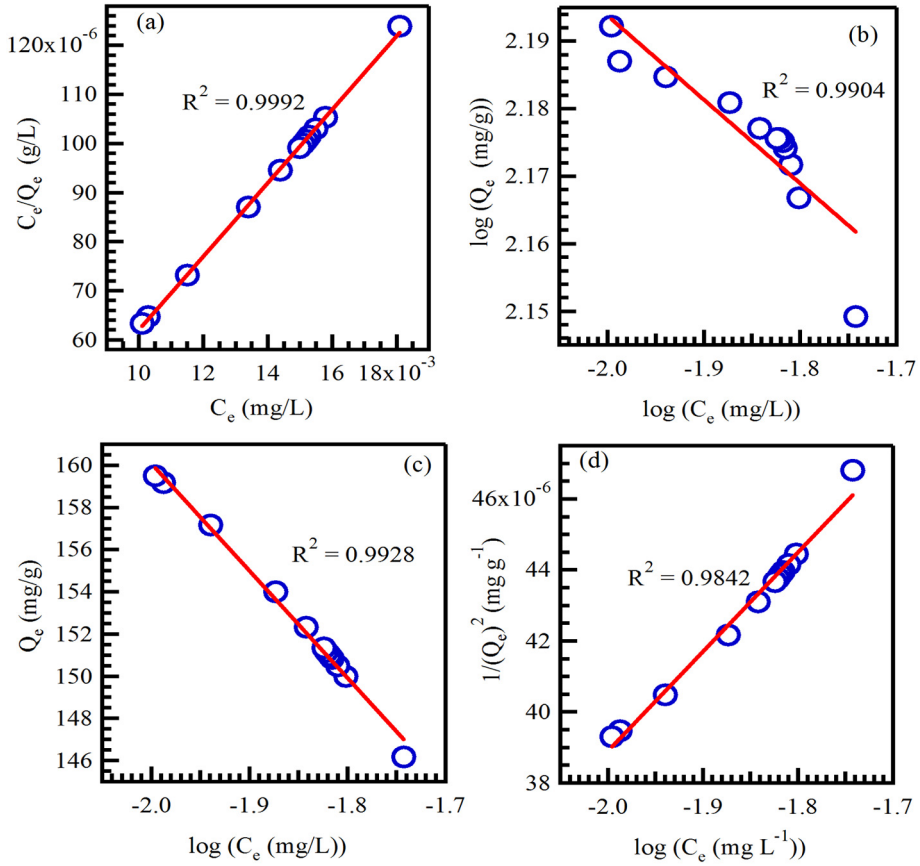

Fig. 6. Adsorption isotherms (a) Langmuir, (b) Freundlich, (c) Temkin and (d) Harkin–Jura for Fe^{3+} ions adsorption onto GO 12 h aerogel.

Table 2
Fitting parameters of Fe^{3+} adsorption experimental data to Langmuir, Freundlich, Temkin and Harkin-Jura isotherm models.

Model	Parameters	R^2
Langmuir	$Q_{max} = 133.33$ mg/g $K_L = 0.57$ L/mg $R_L = 0.01$	0.9992
Freundlich	$1/n = 1.92$ $K_F = 82.77$ mg/g (L/mg)$^{1/n}$	0.9904
Temkin	$B_T = -0.032$ J/mol $K_T = 0.96$ L/g	0.9928
Harkin-Jura	$A_{HJ} = 33.33 \times 10^3$ mg^3/g L $B_{HJ} = 3.00$ mg/L	0.9842

adsorption process where most of the ions are removed at this stage. The adsorption study reveals that GO aerogel with smaller flake size can adsorb more Fe^{3+} ions at a faster rate, which is attributed to its higher surface area to provide higher active sites. Furthermore, GO aerogel with smaller flake size is proven by FTIR analysis to possess higher edge-plane oxygen functionalities which are able to interact with Fe^{3+} ions, as seen at the beginning of the adsorption process. Such phenomenon is schematically illustrated as Fig. 4.

3.3. Adsorption kinetics

The adsorption performance study of GO aerogel continues with the evaluation of adsorption kinetics. The pseudo-first-order and pseudo-second-order models are used in the evaluation study. The mathematical formulas of pseudo-first-order and pseudo-second-order kinetic models are reported elsewhere [26,36,37].

Fig. 5 shows the linear relationships of both kinetic models. From both graphs, the value of q_{cal} (calculated equilibrium of adsorption uptake) is obtained and used for the calculation of normalized standard deviation ($\Delta q\%$). $\Delta q\%$ and the coefficient R^2 are determined to evaluate which kinetics model is fit to describe the adsorption [38]. All calculated kinetic parameters are summarized and compared in Table 1. It is demonstrated that the pseudo-first-order model does not fit to the experimental kinetics data where it is verified by the lower R^2 values. Besides that, the $\Delta q\%$ is comparatively high to indicate the data from the model calculated are different to the experimental data. In contrast, the pseudo-second-order is ideally fit to the experimental kinetics data with high R^2 values and low $\Delta q\%$. Another supporting data for the fitted pseudo-second-order model is the q_{cal} values are very close to q_{exp} values. All the fitting parameters are listed in Table 1. With all these data, there is sufficient evidence to support the adsorption of Fe^{3+} by GO aerogel is fit by the pseudo-second-order kinetics model which suggests the chemisorption is the rate determining step of Fe^{3+} adsorption by GO aerogel as explained by the adsorption mechanism [36,39].

3.4. Adsorption isotherms

The interaction between Fe^{3+} ions and GO aerogel is further investigated by the adsorption isotherm. The equilibrium data are fitted using Langmuir, Freundlich, Temkin and Harkins-Jura models [27,36,39,40].

The maximum adsorption capacity (Q_{max}) and Langmuir constant (K_L) can be calculated from the linear plot as shown in Fig. 6a. Freundlich constant (K_F and 1/n) values can be calculated from the intercept and slope of Fig. 6b. The type of isotherm can be determined according to the value of 1/n. Irreversible isotherm can be determined at ($1/n = 0$). Favorable isotherm can be determined at ($0 < 1/n < 1$). Unfavorable isotherm can be determined at ($1/n > 1$) [10,41]. Using the gas constant value (8.314 J/mol K) and the absolute temperature, Temkin (B_T and K_T) and Harkins-Jura (A_{HJ} and B_{HJ}) constants can be obtained. In this regards, Fig. 6 represents the experimental adsorption data fitted using Langmuir (Fig. 6a), Freundlich (Fig. 6b), Temkin (Fig. 6c) and Harkins-Jura (Fig. 6d) models. The data are fitted by the isotherm models and the corresponding constants are calculated from the intercepts and slopes and listed in Table 2. According to R^2, Langmuir model is the best isotherm model among the others and it means that adsorption of Fe^{3+} onto GO flakes in aerogel is monolayer adsorption onto homogeneous surfaces. These findings are consistent with other metal ions adsorbed on carbon materials [28,36,42,43]. In addition, the calculated separation factor (R_L) [43] value is found to be 0.01 to indicate the adsorption process is favorable. The adsorption capacity of GO 12 h is 133.33 mg/g, as obtained by Langmuir model. This value is higher than all previously reported adsorbent materials for Fe^{3+} removal (Table 3). The findings suggest the potential application of GO aerogel as an adsorbent for Fe^{3+} removal in wastewater treatment.

4. Conclusions

We have demonstrated that GO flake size is an important factor in contributing surface area and edge-plane oxygen functionalities in aerogel. Smaller GO flake size produces aerogel with higher surface area and higher edge-plane oxygen functionalities which can directly enhance heavy metal ions adsorption. Such adsorption is fitted to the pseudo-second-order kinetic model which indicates the chemisorption is the rate-determining step. The Langmuir isotherm model shows the GO aerogel with smaller flake sizes possesses maximum monolayer adsorption capacity of 133.33 mg/g.

Supplementary data to this article can be found online at https://doi.org/10.1016/j.molliq.2018.12.097.

Table 3
Comparison of Fe^{3+} adsorption capacities using some related adsorbents.

Adsorbent	Adsorbate	Adsorption capacity (mg/g)	Ref.
Natural zeolite	Fe^{3+}	6.61	[44]
Hazelnut hull	Fe^{3+}	13.59	[8]
Zeolitic tuff	Fe^{3+}	20.07	[45]
Graphene oxide	Fe^{3+}	27.30	[19]
Chitosan-ethylene glycol diglycidyl ether	Fe^{3+}	46.30	[46]
Chitosan	Fe^{3+}	90.09	[46]
Raw clinoptilolite	Fe^{3+}	98.00	[47]
Sulfonated graphene nanosheets	Cd^{2+}	58.00	[48]
Poly-dopamine/graphene oxide	Pb^{2+}	53.60	[49]
	Cu^{2+}	24.40	
	Cd^{2+}	33.30	
	Hg^{2+}	15.20	
Dithiocarbamate/magnetic reduce graphene oxide	Pb^{2+}	147.06	[50]
	Cu^{2+}	113.64	
	Cd^{2+}	116.28	
	Hg^{2+}	181.82	
Graphene oxide aerogel	Fe^{3+}	133.33	This work

Conflicts of interest

There are no conflicts to declare.

Acknowledgments

The authors would like to acknowledge the funding from the Ministry of Education Malaysia in the form of FRGS [RDU160118: FRGS/1/2016/STG07/UMP/02/3] [RDU170113: FRGS/1/2017/STG07/UMP/01/1] and Universiti Malaysia Pahang grant RDU170357. Moreover, the authors extend their appreciation to King Khalid University, the Ministry of Education – Kingdom of Saudi Arabi for supporting this research through a grant (RCAMS/KKU/002-18) under research center for advanced material science.

References

[1] WHO, Guidelines for Drinking-water Quality: First Addendum to Volume 1, Recommendations, World Health Organization, 2006.
[2] WHO, Progress on Sanitation and Drinking Water: 2015 Update and MDG Assessment, World Health Organization, 2015.
[3] J. García-Martín, R. López-Garzón, M.L. Godino-Salido, M.D. Gutiérrez-Valero, P. Arranz-Mascarós, R. Cuesta, F. Carrasco-Marín, Ligand adsorption on an activated carbon for the removal of chromate ions from aqueous solutions, Langmuir 21 (2005) 6908–6914.
[4] S. Oshiro, M.S. Morioka, M. Kikuchi, Dysregulation of iron metabolism in Alzheimer's disease, Parkinson's disease, and amyotrophic lateral sclerosis, Adv. Pharmacol. Sci. 2011 (2011) 1–8.
[5] R. Selvi, N. Angayarkanni, M. Bharathselvi, R. Sivaramakrishna, T. Anisha, B. Jyotirmoy, B. Vasanthi, Increase in Fe^{3+}/Fe^{2+} ratio and iron-induced oxidative stress in Eales disease and presence of ferrous iron in circulating transferrin, Curr. Eye Res. 32 (2007) 677–683.
[6] V.K. Nguyen, Y. Ahn, Electrochemical removal and recovery of iron from groundwater using non-corrosive electrodes, J. Environ. Manag. 211 (2018) 36–41.
[7] J.S. Kim, L. Zhang, M.A. Keane, Removal of iron from aqueous solutions by ion exchange with Na-Y zeolite, Sep. Sci. Technol. 36 (2001) 1509–1525.
[8] A. Sheibani, M.R. Shishehbor, H. Alaei, Removal of Fe(III) ions from aqueous solution by hazelnut hull as an adsorbent, Int. J. Ind. Chem. 3 (2012) 1–4.
[9] B. Das, P. Hazarika, G. Saikia, H. Kalita, D.C. Goswami, H.B. Das, S.N. Dube, R.K. Dutta, Removal of iron from groundwater by ash: a systematic study of a traditional method, J. Hazard. Mater. 141 (2007) 834–841.
[10] O.A. Habeeb, K. Ramesh, G.A.M. Ali, R.M. Yunus, Low-cost and eco-friendly activated carbon from modified palm kernel shell for hydrogen sulfide removal from wastewater: adsorption and kinetic studies, Desalin. Water Treat. 84 (2017) 205–214.
[11] H. Sadegh, G.A.M. Ali, H.J. Nia, Z. Mahmoodi, Nanomaterial surface modifications for enhancement of the pollutant adsorption from wastewater, in: R. Nazir (Ed.), Nanotechnology Applications in Environmental Engineering, IGI Global, Hershey, PA, USA 2019, pp. 143–170.
[12] H. Sadegh, G.A.M. Ali, Potential applications of nanomaterials in wastewater treatment: nanoadsorbents performance, in: H. Athar, A. Sirajuddin (Eds.), Advanced Treatment Techniques for Industrial Wastewater, IGI Global, Hershey, PA, USA 2019, pp. 51–61.
[13] M. Kobya, E. Demirbas, E. Senturk, M. Ince, Adsorption of heavy metal ions from aqueous solutions by activated carbon prepared from apricot stone, Bioresour. Technol. 96 (2005) 1518–1521.
[14] M. Karnib, A. Kabbani, H. Holail, Z. Olama, Heavy metals removal using activated carbon, silica and silica activated carbon composite, Energy Procedia 50 (2014) 113–120.
[15] X. Ren, J. Li, X. Tan, X. Wang, Comparative study of graphene oxide, activated carbon and carbon nanotubes as adsorbents for copper decontamination, Dalton Trans. 42 (2013) 5266–5274.
[16] H. Sadegh, G.A.M. Ali, V.K. Gupta, A.S.H. Makhlouf, R. Shahryari-ghoshekandi, M.N. Nadagouda, M. Sillanpää, E. Megiel, The role of nanomaterials as effective adsorbents and their applications in wastewater treatment, J. Nanostruct. Chem. 7 (2017) 1–14.
[17] H. Sadegh, Development of graphene oxide from graphite: a review on synthesis, characterization and its application in wastewater treatment, Rev. Adv. Mater. Sci. 49 (2017) 38–43.
[18] O. Moradi, V.K. Gupta, S. Agarwal, I. Tyagi, M. Asif, A.S.H. Makhlouf, H. Sadegh, R. Shahryari-ghoshekandi, Characteristics and electrical conductivity of graphene and graphene oxide for adsorption of cationic dyes from liquids: kinetic and thermodynamic study, J. Ind. Eng. Chem. 28 (2015) 294–301.
[19] W. Konicki, M. Aleksandrzak, E. Mijowska, Equilibrium and kinetics studies for the adsorption of Ni^{2+} and Fe^{3+} ions from aqueous solution by graphene oxide, Pol. J. Chem. Technol. 19 (2017) 120–129.
[20] F. Fang, L. Kong, J. Huang, S. Wu, K. Zhang, X. Wang, B. Sun, Z. Jin, J. Wang, X.-J. Huang, J. Liu, Removal of cobalt ions from aqueous solution by an amination graphene oxide nanocomposite, J. Hazard. Mater. 270 (2014) 1–10.
[21] T.H. Tu, P.T.N. Cam, L.V.T. Huy, M.T. Phong, H.M. Nam, N.H. Hieu, Synthesis and application of graphene oxide aerogel as an adsorbent for removal of dyes from water, Mater. Lett. (2018)https://doi.org/10.1016/j.matlet.2018.1011.1164.
[22] Z. Chen, W. Ren, L. Gao, B. Liu, S. Pei, H.-M. Cheng, Three-dimensional flexible and conductive interconnected graphene networks grown by chemical vapour deposition, Nat. Mater. 10 (2011) 424–428.
[23] X. Mi, G. Huang, W. Xie, W. Wang, Y. Liu, J. Gao, Preparation of graphene oxide aerogel and its adsorption for Cu^{2+} ions, Carbon 50 (2012) 4856–4864.
[24] W.S. Hummers Jr., R.E. Offeman, Preparation of graphitic oxide, J. Am. Chem. Soc. 80 (1958) 1339.
[25] L. Tang, Y. Wang, Y. Li, H. Feng, J. Lu, J. Li, Preparation, structure, and electrochemical properties of reduced graphene sheet films, Adv. Funct. Mater. 19 (2009) 2782–2789.
[26] O.A. Habeeb, K. Ramesh, G.A.M. Ali, R.M. Yunus, Experimental design technique on removal of hydrogen sulfide using CaO-eggshells dispersed onto palm kernel shell activated carbon: experiment, optimization, equilibrium and kinetic studies, J. Wuhan Univ. Technol. Mater. Sci. Ed. 32 (2017) 305–320.
[27] H.H. Abdel Ghafar, G.A.M. Ali, O.A. Fouad, S.A. Makhlouf, Enhancement of adsorption efficiency of methylene blue on Co_3O_4/SiO_2 nanocomposite, Desalin. Water Treat. 53 (2015) 2980–2989.
[28] F.S. Awad, K.M. AbouZeid, W.M.A. El-Maaty, A.M. El-Wakil, M.S. El-Shall, Efficient removal of heavy metals from polluted water with high selectivity for mercury(II) by 2-imino-4-thiobiuret–partially reduced graphene oxide (IT-PRGO), ACS Appl. Mater. Interfaces 9 (2017) 34230–34242.
[29] D.C. Marcano, D.V. Kosynkin, J.M. Berlin, A. Sinitskii, Z. Sun, A. Slesarev, L.B. Alemany, W. Lu, J.M. Tour, Improved synthesis of graphene oxide, ACS Nano 4 (2010) 4806–4814.
[30] G.A.M. Ali, S.A. Makhlouf, M.M. Yusoff, K.F. Chong, Structural and electrochemical characteristics of graphene nanosheets as supercapacitor electrodes, Rev. Adv. Mater. Sci. 40 (2015) 35–43.
[31] L. Stobinski, B. Lesiak, A. Malolepszy, M. Mazurkiewicz, B. Mierzwa, J. Zemek, P. Jiricek, I. Bieloshapka, Graphene oxide and reduced graphene oxide studied by the XRD, TEM and electron spectroscopy methods, J. Electron Spectrosc. Relat. Phenom. 195 (2014) 145–154.
[32] T. Szabó, O. Berkesi, P. Forgó, K. Josepovits, Y. Sanakis, D. Petridis, I. Dékány, Evolution of surface functional groups in a series of progressively oxidized graphite oxides, Chem. Mater. 18 (2006) 2740–2749.
[33] R. Mukherjee, P. Bhunia, S. De, Impact of graphene oxide on removal of heavy metals using mixed matrix membrane, Chem. Eng. J. 292 (2016) 284–297.
[34] M. Pakuła, S. Biniak, A. Świątkowski, Chemical and electrochemical studies of interactions between iron (III) ions and an activated carbon surface, Langmuir 14 (1998) 3082–3089.
[35] A. Tararan, A. Zobelli, A.M. Benito, W.K. Maser, O. Stéphan, Revisiting graphene oxide chemistry via spatially-resolved electron energy loss spectroscopy, Chem. Mater. 28 (2016) 3741–3748.
[36] H. Sadegh, G.A.M. Ali, A.S.H. Makhlouf, K.F. Chong, N.S. Alharbi, S. Agarwal, V.K. Gupta, MWCNTs-Fe_3O_4 nanocomposite for Hg(II) high adsorption efficiency, J. Mol. Liq. 258 (2018) 345–353.
[37] S.M. Seyed Arabi, R.S. Lalehloo, M.R.T.B. Olyai, G.A.M. Ali, H. Sadegh, Removal of Congo red azo dye from aqueous solution by ZnO nanoparticles loaded on multiwall carbon nanotubes, Phys. E. 106 (2019) 150–155.
[38] L. Wang, J. Zhang, R. Zhao, Y. Li, C. Li, C. Zhang, Adsorption of Pb (II) on activated carbon prepared from *Polygonum orientale* Linn.: kinetics, isotherms, pH, and ionic strength studies, Bioresour. Technol. 101 (2010) 5808–5814.
[39] V.K. Gupta, S. Agarwal, H. Sadegh, G.A.M. Ali, A.K. Bharti, A.S. Hamdy, Facile route synthesis of novel graphene oxide-β-cyclodextrin nanocomposite and its application as adsorbent for removal of toxic bisphenol A from the aqueous phase, J. Mol. Liq. 237 (2017) 466–472.
[40] S. Agarwal, H. Sadegh, Monajjemi Majid, A.S.H. Makhlouf, G.A.M. Ali, A.O.H. Memar, R. Shahryari-ghoshekandi, I. Tyagi, V.K. Gupta, Efficient removal of toxic bromothymol blue and methylene blue from wastewater by polyvinyl alcohol, J. Mol. Liq. 218 (2016) 191–197.
[41] H. Sadegh, G.A.M. Ali, Z. Abbasi, M.N. Nadagoud, Adsorption of ammonium ions onto multi-walled carbon nanotubes, Studia UBB Chemia 62 (2017) 233–245.
[42] H. Wang, X. Yuan, Y. Wu, H. Huang, G. Zeng, Y. Liu, X. Wang, N. Lin, Y. Qi, Adsorption characteristics and behaviors of graphene oxide for Zn(II) removal from aqueous solution, Appl. Surf. Sci. 279 (2013) 432–440.
[43] A.B. Dichiara, M.R. Webber, W.R. Gorman, R.E. Rogers, Removal of copper ions from aqueous solutions via adsorption on carbon nanocomposites, ACS Appl. Mater. Interfaces 7 (2015) 15674–15680.
[44] T. Motsi, N.A. Rowson, M.J.H. Simmons, Adsorption of heavy metals from acid mine drainage by natural zeolite, Int. J. Miner. Process. 92 (2009) 42–48.
[45] L. Al-Makhadmeh, M.A. Batiha, Removal of iron and copper from aqueous solutions using Jordanian kaolin and zeolitic tuff, Desalin. Water Treat. 57 (2016) 20930–20943.
[46] W.S.W. Ngah, S. Ab Ghani, A. Kamari, Adsorption behaviour of Fe(II) and Fe(III) ions in aqueous solution on chitosan and cross-linked chitosan beads, Bioresour. Technol. 96 (2005) 443–450.
[47] N.A. Öztaş, A. Karabakan, Ö. Topal, Removal of Fe(III) ion from aqueous solution by adsorption on raw and treated clinoptilolite samples, Microporous Mesoporous Mater. 111 (2008) 200–205.
[48] Y. Shen, B. Chen, Sulfonated graphene nanosheets as a superb adsorbent for various environmental pollutants in water, Environ. Sci. Technol. 49 (2015) 7364–7372.
[49] Z. Dong, D. Wang, X. Liu, X. Pei, L. Chen, J. Jin, Bio-inspired surface-functionalization of graphene oxide for the adsorption of organic dyes and heavy metal ions with a superhigh capacity, J. Mater. Chem. A 2 (2014) 5034–5040.
[50] W. Fu, Z. Huang, Magnetic dithiocarbamate functionalized reduced graphene oxide for the removal of Cu(II), Cd(II), Pb(II), and Hg(II) ions from aqueous solution: synthesis, adsorption, and regeneration, Chemosphere 209 (2018) 449–456.